

CHAPTER 5: PHOTOCATHODE THEORY

JOHN SMEDLEY

*Brookhaven National Laboratory
Upton, NY 11973*

TRIVENI RAO

*Brookhaven National Laboratory
Upton, NY 11973*

DIMITRE DIMITROV

*TechX Corporation
5621 Arapahoe Ave., Suite A
Boulder, CO 80303*

Keywords

Photocathode, Theory of Photoemission, Quantum Efficiency, Three-Step Model, Semiconductor Cathode, Metal Cathode, Diamond Amplifier, Photon Absorption, Electron Excitation, Electron Transport, Electron Emission, Density of States, Transverse Emittance, Schottky Effect, Surface Roughness, Field Enhancement

Abstract

The cathode material used in a photoinjector is chosen to deliver the electron beam parameters for the desired application. Since these parameters at the cathode are determined primarily by the cathode material and the laser, *a priori* calculation of the quantum efficiency (QE) and the intrinsic emittance (IE) at the cathode can be used to compare the theoretical prediction to the observed performance and to improve it. In this chapter, we derive, based on the three step model, the expressions for the quantum efficiency and the intrinsic emittance of the electron beam from the cathode held in high accelerating field. We describe the specific modifications required for calculating these values for the metal, semiconductor and negative electron affinity cathodes. We discuss briefly the impact of surface roughness, impurity and crystal orientation to both the QE and IE. We also describe the theoretical formalism for calculating the electron yield secondary emitters such as diamond, which shows promise for delivering ampere level currents.

One of the primary components in designing photoinjectors is the photocathode to be used for the injector. Several factors dictate this choice: The quantum efficiency of the cathode at the laser's wavelength, the lifetime of the cathode, the total charge deliverable from the cathode in this life time, and its compatibility with the injector. This chapter is devoted to developing the theoretical underpinning of the electron yield from a material and its relevance to the injectors.

5.1 HISTORY

The first publication on photoemission from metals was a study of the photoelectric effect in 1887 [5.1]. Einstein offered the first theory describing the major aspects of this process in 1905 [5.2], work that was mentioned in the citation for his 1921 Nobel Prize. His theory demonstrated the quantization of the energy of light and proposed the existence of a material-dependent escape energy (today called the work function) to explain why UV radiation caused electron emission, but visible light did not. In the century since this groundbreaking work, many advances have been made in studying photoemission. In particular, the advent of lasers allowed the exploration of processes unattainable with less intense light sources, such as multiphoton emission [5.3]. Models of photoemission now describe not only the expected electron yield

from a given metal and light source, but also provide predictions of the energy- and angular-distributions [5.4] of the emitted electrons.

The theory of photoemission relevant to the present work is named the “three-step model” [5.5]–[5.7]. Bergland & Spicer used it to explain emission from several materials [5.8], [5.9]. This model breaks down the process into three independent steps. The first step is the absorption of a photon and the resulting excitation of an electron. The second step is transportation of the excited (hot) electron to the surface; it takes into account the collisions that the electron may undergo during transit. The third step is the escape of the electron from the material after it reaches the surface. Since the three steps are considered to be independent, the probability of a single incident photon generating an emitted electron, defined as the quantum efficiency (QE), is the product of the probability of each of these steps. Although exact calculation of the QE is feasible, it is extremely tedious. Hence, we derive the equation for the QE, making some basic assumptions, and then discuss their validity for different types of cathodes in subsequent sections.

Quantum Efficiency

For these discussions, QE typically is defined as the ratio of the number of emitted electrons (n_e) to the number of incident photons (n_p). We note that this method differs slightly from other treatments [5.8] wherein efficiency is calculated with respect to the absorbed laser energy. For a cathode used in an injector, the incident laser energy generally is known, but the material’s reflectivity may change with the surface preparation technique. Therefore, in these applications, it is standard practice to define the QE with respect to the incident beam’s energy.

$$\text{QE} = \frac{n_e}{n_p} = \frac{h\nu[eV]}{E_{laser}[J]} q [\text{C}] \quad (5.1)$$

where $h\nu$ is the photon energy, q is the charge released by the cathode and E_{laser} is the laser energy.

5.2 THREE-STEP MODEL

5.2.1 Step 1 – Photon Absorption and Electron Excitation

This step entails calculating the probability of a photon being absorbed to excite an electron to a higher energy state. Two assumptions are made in this step. First, that the states lying below the Fermi energy, E_f , are filled and the states above are empty. This is equivalent to treating the material as a conductor at zero temperature. The second is that every absorbed photon excites an electron within the material, with an excitation probability dependent on only three parameters: The photon energy, the number of electrons in the occupied states of the material able to absorb photons (*i.e.* states below E_f), and the number of available states into which the hot electron is excited. The latter assumption, called the random- k approximation, implies that no selection rules are needed based on the electron’s momentum. This simplified version deals only with indirect transitions wherein only the conservation of energy between the photon and the electron is a necessary condition, not the momentum. For polycrystalline metal surfaces typically used as accelerator photocathodes, this is generally a good approximation.

In the first step of the model, two processes occur. The first is the reflection of the incident laser beam from the surface. The probability of transmission into the material, $T(\nu)$, and absorption in an infinitely thick cathode, $A(\nu)$, is calculated from the reflectivity

$$T(\nu) = A(\nu) = 1 - R(\nu) \quad (5.2)$$

The reflectivity of the various materials can be measured or obtained from the literature [5.10]. The depth over which the photons are absorbed is determined by the material's absorption coefficient at $h\nu$.

The second process is the probability of exciting an electron to a given energy within the material. For this treatment, only the kinematic (energy) restrictions are considered. No selection rule is imposed on the wave vector, k , and the momentum matrix elements are assumed constant. This is equivalent to supposing that the electron's transverse momentum is not conserved. This approximation makes the probability of excitation from an initial state of energy E_0 to a final state of energy $(E_0 + h\nu)$ solely a function of the material's electronic density of states (EDOS). For convenience, we take the zero of energy to be the lowest in the material's valence band. The EDOS provide the number of available electron states as a function of energy, $n(E)$. The probability of excitation to a final state $E = (E_0 + h\nu)$, from an initial state E_0 clearly is proportional to the number of initial states, $N(E_0)$, and the number of final states, $N(E)$

$$P(E, h\nu) \propto N(E) N(E_0) = N(E) N(E - h\nu) \quad (5.3)$$

To obtain the fractional number of electrons excited to an energy E , we must divide by the total number of possible transitions

$$\int_{E_f}^{E_f+h\nu} dE' N(E') N(E' - h\nu) \quad (5.4)$$

The lower limit of integration arises from the exclusion principle. There are no empty states below the Fermi level; thus, all excitations must be to states above this level. The upper limit comes from the conservation of energy, as the highest energy initial state has $E = E_f$. Thus we have

$$P(E, h\nu) = \frac{N(E) N(E - h\nu)}{\int_{E_f}^{E_f+h\nu} dE' N(E') N(E' - h\nu)} \quad (5.5)$$

Step one is largely the same for both metallic and amorphous semi-conductor cathodes. The EDOS will be distinct; in particular, the semiconductor will have a band of disallowed states between the highest energy-filled state and the lowest energy-unfilled state. In the special case of spin-polarized photocathodes, the EDOS for each spin state must be considered and a different QE is calculated for each spin orientation.

Cathodes for Polarized Electrons

Currently, the polarized electrons usually are obtained by photoemission from GaAs-based semiconductors [5.11], [5.12]. The primary differences in the theoretical calculation in this case are: a) In addition to energy, the angular and crystal momenta are also conserved during the absorption of photon; and b) the initial and final states are near the absorption edge to reduce electron-phonon (e-p) collisions and preserve the

polarization. Electrons from a specific spin state in the valence band is resonantly excited with circularly polarized light to the final state in the conduction band allowed by the energy and momentum conservation rules. After polarized electrons are generated in the conduction band, they are transported to the emission surface of the semiconductor's photoemitter. This surface is treated to create a negative electron affinity which enhances the emission of electrons.

However, since GaAs is a direct band gap semiconductor and has degenerate heavy-hole- and light-hole-valence bands at the Γ point (the maximum of the valence band), the electrons' spin polarization is limited to 50%. To increase it, degeneracy is removed by using either a strained GaAs layer, or a strained superlattice structure. This splits the sub-bands of the heavy-holes and the light-holes, with the former possessing greater energy than the latter. Electrons are then excited from the heavy-hole band with circularly polarized photons at the absorption edge, as detailed in Chapter 8. The band structure and the EDOS for superlattices usually are calculated using a multi-band Kane model (e.g. [5.13]) that supports the computation of polarization spectra that can be compared [5.11] with spectra from polarized electron emission experiments.

5.2.2 Step 2 – Photon Absorption Length and Electron Transport

The purpose of the second step is to calculate the probability that an excited electron reaches the surface of the cathode while retaining sufficient energy to escape into vacuum. Unlike the first step, this one differs dramatically between metallic- and semiconductor-cathodes.

In both cases, the photon's absorption length, λ_{ph} , in the material determines the depth at which the hot electron is excited. In metallic cathodes, electron-electron (e-e) scattering limits the range of the hot electrons in the material. This is represented by an e-e scattering length, λ_e . Since the theory herein is being developed for "near threshold" emission, a single electron-electron scattering event is likely to remove sufficient energy from the excited electron, such that neither of the electrons involved will retain enough energy to escape from the material. Thus, electrons that undergo a scattering event in the metal are assumed to be lost and not emitted. The e-p scattering in the metal does not change the energy distribution significantly. The momentum transfer due to this scattering is not relevant, since we assume isotropic velocity distribution for the electrons in the initial state; only energy conservation, not momentum conservation, has been taken into account in the transition.

For semiconductor cathodes, if the photon energy used is less than double the band gap energy (Spicer's "magic window"), e-e scattering is forbidden. In this case, other scattering mechanisms dominate (principally e-p). Because these processes entail the interaction of the hot electron with the ion lattice of the semiconductor, they have a small energy transfer, but a large momentum transfer. Therefore, an electron potentially can undergo many scattering events while retaining the energy sufficient to escape. Each event essentially will randomize the electron's direction of travel, leading to the diffusion of carriers to the surface under a random walk. This process typically is treated with a Monte Carlo algorithm with a characteristic scattering length, though other closed-form approaches exist [5.14]. Each scattering event has an associated energy loss and the calculation continues until each excited electron has been emitted or has lost energy such that it cannot overcome the work function. For negative electron affinity materials, charge trapping must also be considered.

5.2.2.1 Detailed Metallic Case

During their journey to the surface, the electrons may undergo a scattering event with an electron, phonon, or an impurity. Only electron-electron interaction is considered here, as its typical scattering length [5.8]

dominates in the energy region of interest, *viz.*, 4-6 eV above the Fermi level. We make several simplifying assumptions herein. We ignore the specifics of the interaction between the excited electron and the “valence” electrons and assume that the probability of the interaction is solely a function of the number of available initial and final states in the material EDOS (the available phase-space for the interaction). Specifically, the probability, S , of an excited electron of energy $E > E_f$ interacting with a valence electron of energy $E_0 < E_f$ and imparting energy ΔE is proportional to:

1. The number of electrons, $N(E_0)$, with energy E_0 .
2. The number of empty states, $N(E_0 + \Delta E)$, with energy $E_0 + \Delta E$.
3. The number of empty states, $N(E - \Delta E)$ with energy $E - \Delta E$.

$$S(E, E_0, \Delta E) \propto N(E_0) N(E_0 + \Delta E) N(E - \Delta E) \quad (5.6)$$

To obtain the total probability of scattering for an electron of energy E by an electron of energy E_0 , we must integrate Equ. 5.6 over all possible energy transfers, ΔE .

$$S(E, E_0) \propto \int_{E_f - E_0}^{E - E_f} d(\Delta E) N(E_0) N(E - \Delta E) N(E_0 + \Delta E) \quad (5.7)$$

The lower limit of integration fulfills the requirement that enough energy must be imparted to the target electron to move it into an unfilled energy state (a state with $E > E_f$). The upper limit requires the initial excited electron retaining enough energy to enter an unfilled state.

To obtain the total scattering probability of an excited electron, we integrate Equ. 5.7 over all possible “valence” electron energies with a lower limit of integration representing the kinematic limitation that $E + E_0 \geq 2E_f$, thereby yielding

$$S(E) \propto \int_{2E_f - E}^{E_f} dE_0 \int_{E_f - E_0}^{E - E_f} d(\Delta E) N(E_0) N(E - \Delta E) N(E_0 + \Delta E) \quad (5.8)$$

The lifetime of the excited state (with respect to e-e scattering), $\tau(E)$, is inversely proportional to this scattering probability [5.15]:

$$\tau(E) \propto \frac{1}{S(E)} \quad (5.9)$$

The scattering length is related to the lifetime by the velocity. Here, we assume that the electron velocity is proportional to the square root of its kinetic energy (as it would be for a nonrelativistic free electron of energy E). The kinetic energy is taken to be the energy above the bottom of the band occupied by the electron for a semiconductor and at the Fermi energy for a metal

$$\lambda_e(E) = v(E) \tau(E) = \frac{\lambda_0 \sqrt{E - E_f}}{\int_{2E_f - E}^{E_f} dE_0 \int_{E_f - E_0}^{E - E_f} d(\Delta E) N(E_0) N(E - \Delta E) N(E_0 + \Delta E)} \quad (5.10)$$

Here, λ_0 is a constant of proportionality that is chosen so that the e-e scattering length (the length over which the intensity of unscattered electrons is $1/e$ of the initial intensity) matches a known value of the electron's mean free path at a single energy for a given material.

The depth at which an electron was excited determines the mean distance that it must travel to reach the surface of the metal. λ_{ph} in the material determines this distance. The absorption length is calculated from the complex index of refraction, $\mathcal{N}^\circ = n + ik$, of the material for each incident wavelength λ [5.10]:

$$\lambda_{ph} = \frac{\lambda}{4\pi k} \quad (5.11)$$

The probability that an electron created at a depth d will escape is e^{-d/λ_e} , and the probability per unit length that a photon is absorbed at depth d is $\lambda_{ph}^{-1} e^{-d/\lambda_{ph}}$. Integrating the product of these probabilities over all possible values of d , we obtain the fraction of electrons that reach the surface without scattering, $T(E, \nu)$,

$$T(E, \nu) = \frac{\lambda_e(E)/\lambda_{ph}(\nu)}{1 + (\lambda_e(E)/\lambda_{ph}(\nu))} \quad (5.12)$$

5.2.2.2 Detailed Semiconductor Case

The number of scattering processes involved complicates the derivation of an analytical expression for electron transport in semiconductor cathodes. As mentioned, the Monte Carlo method often is applied to investigate charge transport in semiconductors. Overall, the method consists of simulating in two main steps, the trajectories of charge particles in an applied field. In the first, the free flight of carriers is calculated by generally solving Maxwell's equations; in the second step, a scattering event is identified (*e.g.* with phonons) and executed with specific probability. For a cathode with minimal field penetration, due to relatively high conductivity (as is typical for GaAs, the alkali antimonides and tellurides), the solution to Maxwell's equations in the bulk leads to (effectively) field-free drift between scattering events. When the energies of conduction electrons and valence holes are sufficiently close to the bottom of the conduction band and the top of the valence band, respectively, only one conduction band and one valence band are used. This Monte Carlo approach to charge transport in semiconductors is reviewed in Chapter 5 of [5.16]. Depending on the energy of absorbed radiation and the energy gap in a semiconductor photocathode, electrons and holes of created electron-hole pairs could have sufficiently large enough energies to produce additional secondary pairs due to impact ionization scattering. This does not occur in standard photocathodes irradiated with near-threshold radiation, but occurs in special cases such as diamond amplified photocathode, described below separately. These free charge carriers then move towards the emission surface *via* diffusion, and also drift when an applied electric field is present. In such a case, the full-band structure approach is used to generally model charge transport.

5.2.3 Step 3 – Escape

Our objective in this section is to calculate the probability that an electron, which has reached the surface, will be moving in the correct direction with sufficient energy to overcome the potential barrier and escape from the cathode's surface. This third step in the model accounts for the direction of travel of the electron as it approaches the surface. To escape, the electron's direction of motion must lie within a cone determined by the electron's energy and the material's work function.

The escape criteria are written [5.4] as

$$\frac{\hbar^2(k_{\perp})^2}{2m} \geq E_T \quad (5.13)$$

where E_T is the energy required to escape ($E_T = \phi$ for a metal). The definition of k_{\perp} we use here differs slightly from others in the literature [5.4]: for us, it represents the component of the excited electron's momentum directed perpendicular to the surface of the cathode material resulting in an escape cone with an opening angle described by [5.17]

$$\cos(\theta) = \frac{k_{\perp min}}{|\vec{k}|} = \sqrt{\frac{E_T}{E - E_f}} \quad (5.14)$$

Here, $k_{\perp min}$ refers to the value of the perpendicular component of the electron momentum for which Equ. 5.13 is an equality representing the minimum perpendicular momentum required to overcome the work function. Only those electrons whose trajectory falls within the cone described by Equ. 5.14 will escape the surface. The excitation and scattering processes are assumed to produce electrons with an isotropic angular distribution. Thus, the fraction of electrons that escape is given by the fraction of the total solid angle subtended by this cone

$$D(E) = \frac{1}{4\pi} \int_0^{\theta} \sin(\theta') d\theta' \int_0^{2\pi} d\varphi = \frac{1}{2} [1 - \cos(\theta)] = \frac{1}{2} \left(1 - \sqrt{\frac{E_T}{E - E_f}} \right) \quad (5.15)$$

The above expression holds as long as $(E - E_f) > E_T$. If $E < E_T$, the electron does not have enough energy to escape the surface, so $D(E) = 0$.

5.2.4 Yield and QE in the Three-Step Model

To calculate the total electron yield from a material for known photon flux I , and photon energy, $h\nu$, we integrate the product of the probabilities calculated in each step:

$$Y(\nu) = I(\nu) A(\nu) \int_{E_T}^{h\nu+E_f} dE P(E) T(E,\nu) D(E) \quad (5.16)$$

Taking the ratio of the electron yield to the incident photon flux, we obtain the QE

$$QE(\nu) = A(\nu) \int_{E_T}^{h\nu+E_f} dE P(E) T(E,\nu) D(E) \quad (5.17)$$

For electrons with energy very close to the threshold for emission ($E - E_T \ll E_T$), the escape cone described in this section represents the dominant factor in determining the energy dependence of the QE [5.4]. In this case, the probability of an electron with energy, E , leaving the metal is proportional only to $D(E)$. The total QE then is proportional to the integral of $D(E)$ over all possible electron energies.

$$QE(\nu) \propto \int_{\phi + E_f}^{h\nu + E_f} D(E) dE \quad (5.18)$$

This integration yields

$$QE(\nu) \propto (h\nu - \phi) + 2\phi - 2\phi \sqrt{1 + \frac{h\nu - \phi}{\phi}} \quad (5.19)$$

Expanding for $(h\nu - \phi) \ll \phi$, and keeping the terms to second order

$$QE(\nu) \propto (h\nu - \phi) + 2\phi - 2\phi \left[1 + \frac{h\nu - \phi}{2\phi} - \frac{1}{8} \left(\frac{h\nu - \phi}{2\phi} \right)^2 \right] \quad (5.20)$$

Collecting the terms, we obtain

$$QE(\nu) \propto (h\nu - \phi)^2 \quad (5.21)$$

Thus, for small values of electron energy in excess of the threshold, we expect the QE to show quadratic dependence on the excess energy.

5.3 THE TRANSVERSE EMITTANCE IN THE THREE-STEP MODEL

The rms transverse emittance in terms of the transverse momentum (referred to as k in material and p in vacuum after emission) and position distributions of the electrons can be expressed as

$$\varepsilon_x = \sqrt{\langle x^2 \rangle \langle x'^2 \rangle - \langle xx' \rangle^2}; \text{ where } x' = \frac{dx}{dz} = \frac{p_x}{p_z} \quad (5.22)$$

If the electrons are accelerated rapidly from rest, the longitudinal momentum p_z reaches relativistic values quickly and can be written as $\beta\gamma mc$; then

$$\varepsilon_x \equiv \frac{1}{\beta\gamma mc} \sqrt{\langle x^2 \rangle \langle p_x^2 \rangle - \langle xp_x \rangle^2} \quad (5.23)$$

If there is no correlation between the position and momentum of the electron, then the cross correlation term vanishes. The normalized emittance can then be written as

$$\varepsilon_n \equiv \beta\gamma \varepsilon_x = \frac{1}{mc} \sqrt{\langle x^2 \rangle} \sqrt{\langle p_x^2 \rangle} = \sigma_x \sigma_{p_x} \quad (5.24)$$

where σ_x is the rms spot size and σ_{p_x} is the dimensionless rms transverse momentum.

The intrinsic transverse momentum distribution of the electrons in the cathode gives rise to an emittance that is characteristic of the cathode material, the photon energy and the external field imposed on the cathode. This can be calculated by determining the variance of the transverse momentum of the electrons exiting the surface.

The product of the probability densities from each of the three steps (prior to energy integration) provides the number of electrons emitted at a given energy from the material. This distribution is called the energy distribution curve (*EDC*).

$$EDC(E,\nu) = A(\nu) P(E) T(E,\nu) D(E) \quad (5.25)$$

As described in Section 5.2.3 and Equ. 5.14, the maximum angle of escape inside the metal, θ_{max} , is given by

$$\cos(\theta_{max}) = \frac{p_z}{p_{total}} = \sqrt{\frac{\phi}{E - E_f}} \quad (5.26)$$

$$p_x = \sqrt{2m(E - E_f)} \sin(\theta) \quad (5.27)$$

where p_x is conserved upon emission. The variance of the transverse momentum can then be written as

$$\sigma_{p_x}^2 = \frac{\int_{E_f}^{h\nu+E_f} \int_0^{\theta_{max}} A(\nu)P(E)T(E,\nu)D(\cos(\theta)) \frac{p_x^2}{(mc)^2} d(\cos(\theta))dE}{\int A(\nu)P(E)T(E,\nu)D(E)} \dots \quad (5.28)$$

$$\dots = \frac{1}{mc^2} \frac{\int_{E_f}^{h\nu+E_f} \int_0^{\theta_{max}} A(\nu)P(E)T(E,\nu)E \sin^2(\theta) d(\cos(\theta))dE}{\int A(\nu)P(E)T(E,\nu)D(E)} \quad (5.28 \text{ cont.})$$

where E is the energy of the electron and θ is the angle between the surface normal and its trajectory inside the cathode. θ_{max} is the angle of the escape cone containing the trajectories of all the electrons and is defined by Equ. 5.14. One should keep in mind that for a NEA surface, for which the vacuum level is below the bottom of the conduction band, $\theta_{max} \approx 90^\circ$ and almost all the electrons reaching the surface escape. The three-step model can be applied to a full energy-momentum band structure calculation, which yields an angle and energy distribution curve. Such a calculation is beyond the scope of this book.

Equ. 5.28 can be simplified following certain assumptions that are valid for a number of cathode materials. If the photon energy is close to the effective work function and the electron density of states near the Fermi energy can be considered a constant, then the above equation can be analytically integrated to result in

$$\sigma_{p_x} = \sqrt{\frac{h\nu - \phi_{eff}}{3mc^2}} \quad (5.29)$$

$$\varepsilon_n = \sigma_x \sqrt{\frac{h\nu - \phi_{eff}}{3mc^2}} \quad (5.30)$$

Experimental results agree with Equ. 5.30, as shown in Chapter 6 and Chapter 7.

5.4 MODIFICATIONS TO THE THREE-STEP MODEL

The previous section addressed the process of photoemission from materials with known properties, *i.e.* EDOS and work function. This section discusses the needed modifications to this model to understand the behavior of the QE of a cathode in a photoinjector. Two major physical characteristics differentiate an electron gun from the “ideal” treatment presented above: The roughness of cathode surface on some scale, which would impact both the charge and the velocity distribution of the electrons and the large electric field (sometimes greater than 100 MV m^{-1}) accelerating the electrons within the gun. In this section, we consider the reduction of the material work function caused by applying an external field (Schottky effect) [5.18], [5.19].

5.4.1 Schottky Effect

This section determines the change in the work function caused by an external electric field. This derivation uses the classical electrodynamic model of work function: the required amount of work to separate a charge from its image within the metal. For our calculations, we treat the cathode surface as a perfect conductor.

In classical electromagnetism, the work function is viewed as arising from the attraction of an electron to its image charge within the metal. In this definition, the work function is the amount of energy required to move an electron from some minimum separation (minimum is undefined in classical theory) to a point at infinity [5.19]. In the absence of an applied field, the potential energy between an electron at a distance from the surface of a perfect conductor, x , and its image charge is

$$W_{e-image}(x) = e\Phi_{image}(x) = e\left(\frac{-e}{2x}\right) \quad (5.31)$$

To avoid unnecessary constants and remain true to the reference material, this derivation is performed in CGS units. However, the result is stated in MKSA units.

By symmetry, the potential energy between the electron and the surface is half of this value:

$$W_{surface}(x) = \left(\frac{-e^2}{4x}\right) \quad (5.32)$$

The work function then is

$$\phi_0 = W_{surface}(\infty) - W_{surface}(x_{min}) = \left(\frac{e^2}{4x_{min}} \right) \quad (5.33)$$

Now, let us add the effect of an applied field at the surface. The potential corresponding to a constant electric field normal to the surface is

$$W_{field}(x) = e\Phi_{field}(x) = e(-Ex) \quad (5.34)$$

Here, E is the magnitude of the electric field that is normal to the surface of the conductor. The total potential energy then is

$$W_{total}(x) = \left(\frac{-e^2}{4x} \right) - eEx \quad (5.35)$$

This combined potential has a maximum below vacuum level, which occurs at x_0 , such that

$$\frac{d}{dx}W_{total}(x)|_{x=x_0} = \frac{e^2}{4x_0^2} - eE = 0 \quad (5.36)$$

$$x_0 = \frac{1}{2}\sqrt{\frac{e}{E}} \quad (5.37)$$

$$W_{total}(x_0) = -e\sqrt{eE} \quad (5.38)$$

This maximum represents a change in the work function due to the applied field

$$\phi = W_{total}(x_0) - W_{total}(x_{min}) = \frac{e^2}{4x_{min}} - e\sqrt{eE} \quad (5.39)$$

Here, we assume that x_{min} is so close to the surface that $W_{field}(x_{min}) = 0$. This change in the work function is called the Schottky effect. In MKSA units

$$\Delta\phi_{Schottky} [\text{eV}] = \alpha\sqrt{E \left[\frac{\text{V}}{\text{m}} \right]} \quad (5.40)$$

$$\alpha = e\sqrt{\frac{e}{4\pi\epsilon_0}} = 3.7947 \times 10^{-5} [e\sqrt{\text{Vm}}]$$

The modified work function is then

$$\phi = \phi_0 - \alpha\sqrt{E} \quad (5.41)$$

In the presence of an external applied field that modifies the work function from ϕ_0 to ϕ , Equ. 5.20 can be written as

$$QE(v) \propto (hv - \phi_0 + \alpha\sqrt{E})^2 \quad (5.42)$$

$$\sqrt{QE(v)} = A(hv - \phi_0 + \alpha\sqrt{E}) \quad (5.43)$$

where A is a constant of proportionality. This expression predicts a linear relationship between \sqrt{QE} and \sqrt{E} ; this prediction will be important in analyzing the experimental data in the following chapters.

5.4.2 Effect of Surface Roughness

The preceding analysis assumes that the field at the surface of the conductor is uniform and equal to the field in the center of the space between the electrodes, as is true for flat, idealized surfaces. Studies of field emission [5.21], [5.22] demonstrated that micro-protrusions and surface contaminants can effectively enhance the field at the emitting surface. In analyzing field emission curves (charge versus field), it is customary to introduce a factor β_{FE} (the field enhancement factor) that multiplies the applied field to obtain the surface field; enhancement factors of 20-100 for field emission are common in the literature [5.23]. We note that some authors [5.22], [5.24] attributed the large “enhancement” to factors other than the emitter’s geometry, such as non-metallic inclusions in cracks or grain boundaries. These enhancements generally do not impact the calculation of quantum efficiency significantly for a planar geometry. This is due to Gauss’s law – unlike field emission, photoemission occurs over the entire illuminated surface. Surface non-uniformity leads to field enhancement in some areas and field reductions in others. The net effect on the calculation of quantum efficiency is negligible; indeed when a field enhancement factor is introduced into Q versus field plots for photoemission, β is invariably found to be near one.

An exception to this occurs when a cathode is illuminated with a photon energy below (but close to) the work function. In this case, the Schottky effect is required for any emission at all and the cathode will emit only from areas where the field is sufficiently enhanced to reduce the local work function below the photon energy. In this case the field enhancement factor will be a function of the photon energy used. Another exception occurs in the case of needle cathodes, where the field is enhanced over the entire needle tip and only the tip is illuminated. In these cases, a field enhancement factor for photoemission, β_{PE} , is sometimes introduced in front of E in Equ. 5.41 – however, it should be noted that this is an approximation, as the field enhancement strictly applies only to a microscopic treatment of the surface, and therefore the enhancement should be $\beta(x,y)$, where β is allowed to freely vary from point to point along the surface.

More important than the impact on the QE is the impact of surface roughness on the intrinsic emittance. The modification of the applied field at the microscopic photoemission sites has a number of implications to the intrinsic emittance of the electrons from the cathode: initial energy, transverse velocity and charge density of the emitted electrons become spatially dependent.

5.4.3 Effect of Field Enhancement on Emittance

On a macroscopic scale, the applied field is normal to the cathode surface. However, within a few nanometers of the surface, the field lines are normal, not to the macroscopic surface, but the microscopic contour of the surface. As described earlier, this results in a spatially dependent change in the work function and a corresponding spatially dependent charge density. This is shown schematically in Figure 5.1. This change in the work function also gives rise to a spatially dependent excess energy as the electrons exit the

cathode. In addition, once emitted, these low energy electrons follow the local field lines, leading to a spatially dependent velocity distribution transverse to the beam axis.

As can be seen from Equ. 5.28 and Equ. 5.43, the normalized emittance varies as the effective work function and the field distribution change from the peak to the valley of the rough cathode surface. One should keep in mind the θ occurring in Equ 5.28 refers now to the microscopic surface. The net effect of this variation is to introduce a dependence of the intrinsic emittance on the amplitude (n) and spatial period (d) of the roughness, and on the electric field. This effect can be characterized by a "roughness" parameter $\xi = 2\pi n d^{-1}$; a parameter of unity results in a significant ($\sim 30\%$) increase in the expected intrinsic emittance for reasonable fields (24 MV m^{-1}). [5.25] [5.26]

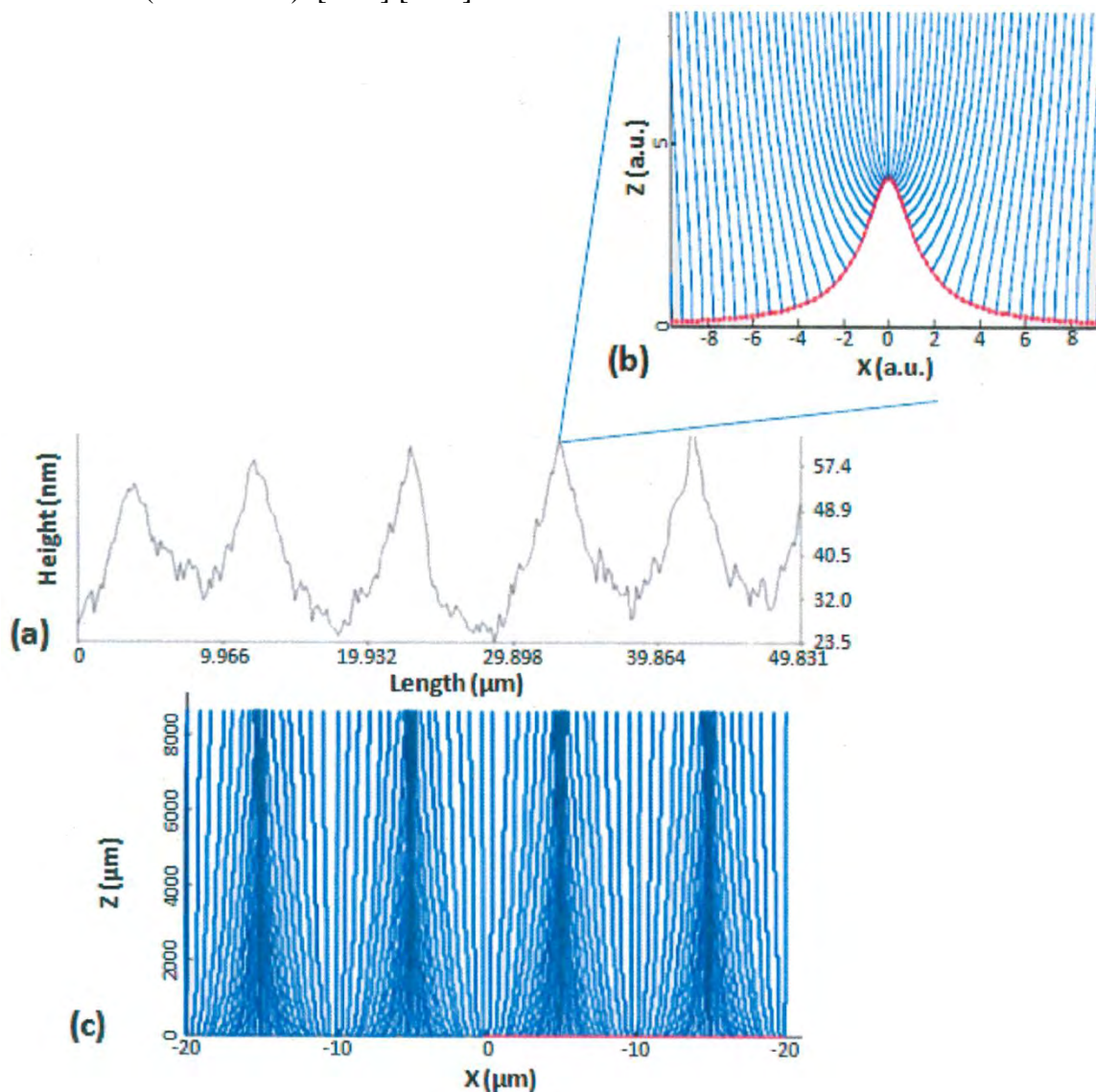


Figure 5.1. a) Surface roughness of a copper cathode used in LCLS injector; b) distribution of field lines in the vicinity of one of the protrusions; c) distribution of the photoemitted charge in the vicinity and a few mm away from the cathode, indicating position dependent transverse velocity dependence in the vicinity of the cathode. [5.27]

In addition to the microscopic protrusions, the roughness of the cathode could be caused by other effects such as random orientation of the crystalline cathode or impurities embedded in or on the cathode: all of these effects lead to non-uniform charge density at or near the cathode surface.

5.5 DIAMOND AMPLIFIER THEORY

A new concept (a diamond amplifier photocathode) to emit high average current, high brightness electron beams was proposed recently, and is currently being developed [5.28]. The underpinning of its operation is to first generate a primary beam of electrons (accelerated to ~ 10 keV) using a conventional photocathode and inject them into a diamond, with its entrance face coated with a metal. The energetic primary electrons scatter inelastically in the diamond, generating (through impact ionization) a number of secondary electrons and holes. These secondary electrons and holes initially relax their energies by producing more electron-hole pairs *via* impact ionization. When the energy of these free charge carriers closely approaches the energy gap value of diamond, scattering by phonons thereafter dominates the further relaxation of their energy. These free charge carriers then move towards the emission surface *via* diffusion and also drift when an applied electric field is present. In such a case, the full-band structure approach is used to generally model charge transport. Algorithms for full-band structure charge transport calculations are detailed in [5.16].

Investigating these phenomena requires modeling of the generation of secondary electrons, charge transport and electron emission.

Secondary electron generation (impact ionization) is treated using optical models (*e.g.* [5.29] and references therein). Where it is allowed, impact ionization continues until the energies of the free (conduction band) electrons and holes in the valence band fall below the energy gap. The scattering rate (or the mean-free-path) for impact ionization in semiconductors [5.29] of interest is such that the impact ionization is completed within several hundred femtoseconds. Modeling the impact ionization is important to understand when the free charge carriers are created (with the process initiated by primary electrons with energies of a few kiloelectron volts) near the metalized side of the amplifier [5.28] and then transported to its emission surface. Electrons recombine at the metal contact due to diffusive expansion, thereby reducing the total number of free electrons that reach the emission surface.

After the impact ionization phase is completed, (or electron-hole pairs created with energies below the energy gap,) the charge carriers drift under an applied electric field and scatter predominantly with lattice excitations (phonons). Scattering with charge impurities and trapping effects must also be accounted for when the densities of charge impurities and trapping centers are not negligible [5.30]. Trapping of charge carriers also leads to the modification of the effective field in diamond, which in turn, affects the transport of free electrons and holes. Both impact ionization and charge transport-related scattering processes are treated *via* Monte Carlo methods.

The emission of electrons from diamond requires modeling surface phenomena that include calculating the probability for emission, band bending, electron affinity, surface roughness and charge-trapping effects.

5.6 CONCLUSION

In this chapter, we have described the theoretical underpinning of the photoemission process, namely the three-step model, and developed the equations relevant to calculate the quantum efficiency of the cathode in a photoinjector. These can be used to evaluate the expected performance of the cathode in the injector, its optimization and even engineer the appropriate cathode using modern material science techniques. We also describe the modification to the model due to Schottky effect when operating the cathodes in the presence of high accelerating fields and its effect on the work function and quantum efficiency. We have derived the

intrinsic emittance of the electrons arising from the transverse momentum distribution at birth, its relationship to the quantum efficiency and the impact of surface roughness on all these parameters.

5.7 CONFLICT OF INTEREST AND ACKNOWLEDGEMENT

We confirm that this article content has no conflicts of interest and would like to acknowledge the supported of US department of Energy under contract numbers DOE DE-SC0003965, DE-AC02-98CH10886, KC0407-ALSJNT-I0013 and DE-FG02-12ER41837.

References

- [5.1] H. Hertz, "Ueber einen einfluss des ultravioletten lichtetes auf die electriche entladung," *Annalen Physik*, vol. 267, pp. 983-1000, 1887.
- [5.2] A. Einstein, "Über einen die erzeugung und verwandlung des lichtetes betreffenden heuristischen gesichtspunkt," *Annalen Physick*, vol. 17, pp. 132-148, 1905.
- [5.3] G. Farkas, A. Kohazi-Kis and C. Toth, "Above-threshold multiphoton photoelectric effect of a gold surface," *Optical Eng.*, vol. 32, pp. 2476-2480, October 1993.
- [5.4] M. Cardona and L. Ley, Eds., *Photoemission in Solids: General Principles*, vol. 1, Berlin: Springer-Verlag, 1978, pp. 22-2, 237-264.
- [5.5] H. Y. Fan, "Theory of photoelectric emissions from metals," *Phys. Rev.*, vol. 68, pp. 43-52, July 1945.
- [5.6] H. Mayer and H. Thomas, "Zum äußeren lichtelektrischen effekt der alkalimetalle. II. Die spektrale verteilung der quantenausbeute bei kalium," *Zeitschrift Physik A*, vol. 147, pp. 419-441, August 1957.
- [5.7] H. Puff, "Zur theorie der photoelektronenemission von metallen. II. Die verteilungen der photoelektronen," *Physica Status Solidi (b)*, vol. 1, pp. 704-715, 1961.
- [5.8] W. F. Krolikowski, Ph.D. thesis, Stanford University, Stanford, CA, USA, 1967.
- [5.9] C. N. Berglund and W. E. Spicer, "Photoemission studies of copper and silver: theory," *Phys. Rev. A*, vol. 136, pp. A1030-A1044.
- [5.10] *CRC Handbook of Chemistry and Physics*, 65th Ed., CRC Press., Boca Roton, Fl, 1984, pp. E-365.
- [5.11] A. V. Subashiev, L. G. Gerchikov and A. N. Ipatov, "Optical spin orientation in strained superlattices," *J. Appl. Phys.*, vol. 96, pp. 1511-1520, August 2004.
- [5.12] T. Nishitani, T. Nakanishi, M. Yamamoto *et al.*, "Highly polarized electrons from GaAs-GaAsP and InGaAs-AlGaAs strained-layer superlattice photocathodes," *J. Appl. Phys.*, vol. 97, pp. 094907-1–094907-6, April 2005.
- [5.13] L.C.L.Y. Voonand and M. Willatzen, *The k-p Method: Electronic Properties of Semiconductors*, Springer-Verlag, 2009.
- [5.14] K. L. Jensen, B. L. Jensen, E. J. Montgomery *et al.*, "Theory of photoemission from cesium antimonide using an alpha-semiconductor model," *J. Appl. Physics*, vol. 104, pp. 044907-1–044907-10, August 2008.
- [5.15] D. Griffiths, *Introduction to Elementary Particles*, John Wiley & Sons, 1987, pp. 194-195.
- [5.16] C. Jungemann and B. Meinerzhagen, *Hierarchical Device Simulation, The Monte-Carlo Perspective*, Chapter 5, New York: Springer-Verlag, 2003.
- [5.17] N. V. Smith, "Photoemission properties of metals," *Crit. Rev. Solid State Material Sci.*, vol. 2, pp. 45-83, 1971.
- [5.18] W. Schottky, "Über den austritt von elektronen aus glühdrähten bei verzögernden potentialen," *Annalen Physik*, vol. 44, pp. 1011-1032, 1914.
- [5.19] C. Herring and M. H. Nichols, "Thermionic emission," *Rev. Modern Physics*, vol. 21, pp. 185-271.
- [5.20] J. D. Jackson, *Classical Electrodynamics*, New York: John Wiley & Sons, 1962, pp. 45, 60.

An Engineering Guide to Photoinjectors, T. Rao and D. H. Dowell, Eds.

- [5.21] R. H. Fowler and L. Nordheim, "Electron emission in intense electric fields," in *Proc. Royal Society A*, vol. 119, May 1928, pp. 173-181.
- [5.22] G. A. Mesyats and D. I. Proskurovsky, *Pulsed Electrical Discharge in Vacuum*, Heidelberg: Springer-Verlag, 1989.
- [5.23] P. A. Chatterton, "A theoretical study of field emission initiated vacuum breakdown," in *Proc. Physical Society*, vol. 88, 1966, pp. 231-245.
- [5.24] R. V. Latham, "The origin of prebreakdown electron emission from vacuum-insulated high voltage electrodes," *Vacuum*, vol. 32, 1982, pp. 137-140.
- [5.25] M. Krasilnikov, "Impact of the cathode roughness on the emittance of an electron beam," in *Proc. 2006 Free Electron Laser*, 2006, pp. 583-586.
- [5.26] D. Xiang, W.-H. Huang, Y.-C. Du *et al.*, "First principle measurements of thermal emittance for copper and magnesium," in *Proc. 2007 Particle Accelerator Conf.*, 2007, pp. 1049-1051.
- [5.27] D. H. Dowell, private communication.
- [5.28] X. Chang, Q. Wu, I. Ben-Zvi *et al.*, "Electron beam emission from a diamond-amplifier cathode," *Phys. Rev. Lett.*, vol. 1054, pp. 164801-1–164801-4, October 2010.
- [5.29] B. Ziaja, R. A. London and J. Hajdu, "Ionization by impact electrons in solids: Electron mean free path fitted over a wide energy range," *J. Appl. Phys.*, vol. 99, pp. 033514-1–033514-9, February 2006.
- [5.30] M. Lundstrom, *Fundamentals of Carrier Transport*, 2nd ed., Cambridge: Cambridge University Press, 2000.